First-principles study of point defects under varied chemical potentials in Li_{4}BN_{3}H_{10}

David E. Farrell and C. Wolverton

Phys. Rev. B **85**, 174102 — Published 1 May 2012

DOI: 10.1103/PhysRevB.85.174102

First-Principles Study of Point Defects Under Varied Chemical Potentials in $Li_4BN_3H_{10}$

David E. Farrell and C. Wolverton*

Electrification Research and Advanced Engineering

Ford Motor Company, Dearborn, MI USA and

Dept. of Materials Science and Engineering

Northwestern University, Evanston, IL USA

(Dated: April 18, 2012)

Abstract

We have employed density functional theory calculations to determine the formation energy for a number of neutral and charged point defects in the mixed anion hydrogen storage compound $Li_4BN_3H_{10}$, under a variety of chemical potentials, to investigate the possible role of point defects in hydrogen desorption. We discuss the determination of chemical potentials based on four-phase equilibria that arise from the temperature dependent decomposition reactions. Our results indicate the following: 1) Neutral NH vacancies are nearly always the lowest energy defect, and have a small positive formation energy up to the experimental hydrogen desorption temperature. 2) The cases where NH vacancies are not the lowest energy correspond to unstable four-phase equilibria. 3) Separated pairs of oppositely charged defects are always higher energy than the analogous combined neutral defect.

PACS numbers: 61.20.Ja

Keywords: hydrogen storage, point defect, vacancy, interstitial, complex hydride, lithium boron nitrogen hydrogen

I. INTRODUCTION

The search for a viable alternative to fossil fuels in automobiles has led to much work in the area of efficient, high-capacity hydrogen storage systems[1,2]. Complex hydrides[3,4] have the possibility of providing high gravimetric and volumetric hydrogen storage densities in a solid-state material, making them an attractive basis for on-board fuel-cell systems. However, the use of these materials is not without its challenges, particularly in the area of hydrogen absorption/desorption kinetics.

$Li_4BN_3H_{10}$ is a complex hydride that was found experimentally to have a high hydrogen capacity, releasing greater than 10 wt. % H_2[5] making it of interest for vehicular applications. A number of experimental studies have focused on the decomposition[5–7], structure[6,8,9] and phase stability[10] of the compound. Thermodynamics predicts favorable hydrogen desorption reactions for all temperatures[11] while experiments in both the pristine[5,6] and catalyzed[7] material found that hydrogen and ammonia release occurred only at temperatures well above room temperature, indicating that the desorption reactions in this system are kinetically limited. At temperatures where the compound remains crystalline, point defect formation and migration is responsible for mass transport and may play an important role in chemical reaction mechanisms. A more complete understanding of the role of point-defect mediated mechanisms for hydrogen desorption is desirable, as the authors are unaware of any experimental work that elucidates the prevalent defects or defect-based mechanisms in $Li_4BN_3H_{10}$. A necessary first step to understanding the role of defects in this material is to obtain accurate data on the energetics and stability of native defects under chemical conditions that may arise during desorption. Here, we perform such a study using a computational approach via Density Functional Theory (DFT).

Density Functional Theory based calculations have been widely used to predict and explore the structure, vibrational properties and thermodynamics of a number of hydrides[2,12–17] including complex hydrides such as $LiBH_4$[18], $NaAlH_4$[19,20], $LiNH_2$[21], Li_2NH[22,23], $Ca(AlH_4)_2$[24], $Li_2Mg(NH)_2$[25], $Ca(BH_4)_2$[26], $Li_4BN_3H_{10}$[7,11,27–29], $Mg(BH_4)_2$[30,31], $Ca(BH_4)_2$-$Mg(BH_4)_2$[32], $(NH_4)_2B_{12}H_{12}$[33], $Li_6Mg(NH)_4$[34], rare-earth aluminum hydrides[35], the Li-Sc-B-H[36], Li-Mg-N-H[37] and Li-Zn-B-H systems[38], and metal-$B_{12}H_{12}$ compounds[39,40]. Of direct importance to this work, DFT has been applied to study native defect formation energies and metal additives in complex hydrides such as $NaAlH_4$[41–46], $LiBH_4$[45], $Mg(NH_3)_nCl_2$[47] and the formation

energy of hydrogen-related defects in AlH_3[48], $CaBH_4$[49], and $Li_4BN_3H_{10}$[50].

Work performed by Hoang and Van De Walle[50] provided insight into the energetics of hydrogen vacancies, hydrogen interstitials, and transition metal impurities in $Li_4BN_3H_{10}$. They examined the energetics of charged and neutral defects, using DFT and a set of chemical potentials defined by a four-way equilibrium between $Li_4BN_3H_{10}$, NH_3, Li_2NH and Li_3BN_2. They found that the lowest energy hydrogen related defects are charged, and therefore have Fermi-level dependent formation energies. From their results, it can be inferred that a pair of separated oppositely charged hydrogen interstitials (i.e., interstitial H^+ and H^- far from one another) should be the lowest energy neutral hydrogen defect. However, even with this prior work, several open questions still remain, such as: 1) How do other vacancy types compare with the hydrogen defects? 2) How are the point defect energetics and stability affected by different chemical potentials and temperatures? and 3) What set(s) of chemical potentials correspond to the experimental and thermodynamically predicted decomposition reactions?

To address these questions, we made use of plane-wave DFT to calculate the formation energy for a variety of vacancies as well as hydrogen interstitials in $Li_4BN_3H_{10}$ through a range of chemical potentials. We formulated five different sets of temperature dependent chemical potentials based on various local equilibrium conditions. In addition, we consider the chemical potentials used in Ref. 50 for the sake of comparison. We find that neutral NH vacancies are the lowest energy defect for nearly all of our local equilibrium conditions and temperatures. For the cases where the NH vacancy is not the lowest, the lowest energy defect is a neutral BH_3 vacancy with a negative formation energy. However, a negative formation energy would result in an instability in the system with spontaneous formation of defects. Therefore, negative formation energies indicate that the assumed local equilibrium conditions are not realistic. Finally, we find that separated pairs of oppositely charged defects are always higher energy than the analogous combined neutral defect.

II. METHODOLOGY

A. Density Functional Theory

Our calculations were carried out with the Vienna Ab Initio Simulation Package (VASP[51–55]) plane-wave DFT code. We use the Perdew-Wang 1991 (PW-91) generalized gradient approximation (GGA)[56], Blöchl's projector augmented wave (PAW) method[55,57] for core-valence electron interactions, and a (2x2x2) Monkhorst-Pack k-point grid. We employed a Gaussian smearing scheme for the electronic occupancies, with a width of 0.1 eV. For H,B and N, we included the outermost orbitals (1s and 2s2p orbitals, respectively) in our calculation while for Li we included 1s semicore states as valence, with an overall energy cutoff of 520 eV for all calculations. We chose a 10^{-4} eV electronic convergence criteria and a .001 eV ionic relaxation convergence criteria. These parameters are similar to those used in previous studies[11,29], though we used a higher energy cutoff than that used in Ref. 50 and made use of an energy-based rather than force-based ionic convergence criterion. However, we found the forces in our calculations to be less than ~ 0.05 eV/Å, which we considered sufficiently converged for our purposes.

B. Types of Defects Considered

The 144 atom (8 formula unit) conventional cell of $Li_4BN_3H_{10}$, shown in Figure 1, based on experimental data[6](then relaxed via DFT) served as our initial defect-free reference geometry. For each defect type we added or subtracted the appropriate atoms from the reference system, specified the number of electrons and relaxed the atomic positions in the structure while keeping the lattice parameters constant. This is the same procedure employed by Hoang and Van de Walle[50], and is intended to mimic the defect being isolated in the bulk material. In the BH_4^- and NH_2^- vacancy cases, we used a (2x2x2) supercell containing 1152 atoms, because of the the value of the electrostatic interactions between images was significantly larger in the 144 atom cells, while this was not the case with the Li^+ vacancy. As a result, we assumed the 144 atom cell was large enough for the smaller charged vacancies. For the H and H_2 vacancies, we considered multiple configurations to examine how the local environment may affect the formation energy. For H vacancies, we considered each of the 4 symmetrically inequivalent positions (Figure 1), referred to here

as 'H1', 'H2', 'H3', and 'H4'. For the H_2 vacancies we considered 2 cases: configuration 1 where 2 'H2' atoms were removed from neighboring NH_2^- anions and configuration 2 where an 'H1' and an 'H4' atom were removed from neighboring NH_2^- and BH_4^- anions.

For H interstitials, we performed an 'exhaustive' search for the lowest energy interstitial position for each charge state (i.e., neutral and ± 1 e^-). Our search involved a group of relaxations with the H atom in one of 70 different starting locations within the periodic cell. We determined the locations by discretizing the cell using a uniform grid, placing H atoms at the grid points and discarding those configurations where H atoms were within .5 Å of another atom. We relaxed each of these configurations individually for each charge state. The resulting relaxed defect configurations for each charge state consisted of energetically degenerate defects at discrete energy levels, including several at the lowest energy, leading us to conclude that our search likely contained the lowest energy configuration. For brevity, we report only the lowest energy H interstitial configurations for each charge state in our discussion.

In the NH vacancy cases, we considered 2 configurations: configuration 1 where an N and 'H2' atom were removed from one NH_2^- anion and configuration 2 where an N and 'H1' atom were removed from one NH_2^- anion. For the remainder of the defects only one configuration was considered. In the case of the $LiBH_4$ and $LiNH_2$ vacancies, the Li^+ and BH_4^- or NH_2^- ions removed were nearest neighbors. For BH_3, the B and three 'H3' atoms were removed from a single anion. Meanwhile for the NH_3 vacancy, an NH_2^- anion and a nearby 'H1' atom were removed. To create the BN vacancy, the B and N atoms removed were from neighboring anions. Finally, for the LiH vacancy an Li^+ cation and a nearby 'H3' atom were removed. We have summarized the various vacancy configurations we considered in Table I.

C. Defect Formation Energies

Once each structure has been relaxed and the total energy at 0 K (i.e. excluding zero-point phonon contributions) obtained, the defect formation energy can be calculated from the following equation[58]:

$$E^f[X^q] = E_{tot}[X^q] - E_{tot}[\mathrm{Li_4BN_3H_{10}}, bulk] - \sum_i n_i \mu_i + q(E_F + \Delta V) \qquad (1)$$

Vacancy Type		Atom Types Removed
Neutral	BH_3	B and H3-type H atoms removed from the same anion
	NH_3	NH_2^- anion and nearby H1-type H atom (from an NH_2^-)
	LiH	Li^+ cation and nearby H3-type H atom (from a BH_4^-)
	BN	B and N atom removed from adjacent anions
	$LiBH_4$	Li^+ cation and nearest neighbor BH_4^- anion
	$LiNH_2$	Li^+ cation and nearest neighbor NH_2^- anion
	H_2 config 1	2 H2-type H atoms from nearest neighbor NH_2^- anions
	H_2 config 2	H1-type and H4-type H atoms from neighboring NH_2^- and BH_4^- anions
Both	H1	H1-type H atom (from an NH_2^-)
	H2	H2-type H atom (from an NH_2^-)
	H3	H3-type H atom (from a BH_4^-)
	H4	H4-type H atom (from a BH_4^-)
	NH config 1	N and H2-type H atoms from one NH_2^- anion
Charged	Li^-	an Li^+ cation
	BH_4^+	a BH_4^- anion
	NH_2^+	an NH_2^- anion

TABLE I. Summary of vacancy types and which type of atoms were removed. H1, H2, H3 and H4 refer to the symmetrically inequivalent hydrogen sites illustrated in Figure 1.

Where $E_{tot}[X^q]$ denotes the DFT static energy of a defect with charge state q (i.e. formal charge of the defect), $E_{tot}[Li_4BN_3H_{10}, bulk]$ denotes the energy of defect-free bulk $Li_4BN_3H_{10}$, n_i denotes the number of atom type i added (n_i is negative if atoms are removed) and μ_i is the chemical potential for atom type i. The final term (in parentheses) in Equation 1 represents the chemical potential for the electrons, where E_F denotes the Fermi energy relative to the energy at the valence band maximum (VBM) of the perfect crystal and q is the charge of the defect. The term ΔV is a so-called 'potential alignment term', and accounts for the shift in the electrostatic potential between the perfect crystal and the system with a defect in a finite simulation cell. Following the procedure used by Van de Walle and Neugebauer[58], we defined the potential alignment term as the difference between the electrostatic potential

in the system with a defect and the perfect crystal. Our reference point for this difference was the point furthest from the center of the defect in the periodic cell. We found that the value of this alignment term varied between defect types, with magnitudes of approximately 0.2-0.9 eV.

D. Choice of Chemical Potentials

In our $Li_4BN_3H_{10}$ system, there are four chemical potentials, one per species ($\mu_{Li}, \mu_B, \mu_N, \mu_H$), that need to be defined. For purposes of comparison to the earlier work of Hoang and Van de Walle[50], we made use of the chemical potentials described in their paper. As their paper did not specify the structure used to calculate the energy of Li_2NH, we chose to use the structure published by Mueller *et al.*[23]. However, we also wished to examine the influence of varied chemical potentials, specifically those that may arise during hydrogen desorption. Therefore, we must assume that there exists some local four-phase equilibrium that will allow us to define the chemical potentials under possible desorption conditions.

For each local equilibrium, we assumed that the system was in equilibrium with $Li_4BN_3H_{10}$, H_2, and two other species. To obtain guidance for the choice of these other species, we consider the thermodynamically favored desorption reactions for $Li_4BN_3H_{10}$[11]:

$$Li_4BN_3H_{10} \rightarrow 2\ LiNH_2 + 2\ LiH + BN + 2\ H_2 \qquad (0\ K \leq T \leq 300\ K) \qquad (A)$$

$$Li_4BN_3H_{10} \rightarrow \quad Li_3BN_2 + LiNH_2 + 4\ H_2 \qquad (300\ K < T \leq 700\ K) \qquad (B)$$

$$Li_4BN_3H_{10} \rightarrow Li_3BN_2 + LiH + \tfrac{1}{2}\ N_2 + \tfrac{9}{2}\ H_2 \qquad (700\ K < T) \qquad (C)$$

For reaction B, the decomposition pathway observed[5] at 520 K, the selection process for the remaining species appears straightforward as there are only two other species in the reaction (Li_3BN_2 and $LiNH_2$) that could be used to set up a four-phase equilibrium. There is a problem with this straightforward approach: the resulting equations for the four-phase equilibrium associated with reaction B are linearly dependent and thus a unique solution for all four chemical potentials is not possible.

Envision a two interface model such as that shown in Figure 2[41]. Here, we imagine bulk $Li_4BN_3H_{10}$ in separate thermodynamic equilibrium with $LiNH_2$ and H_2 at one interface and Li_3BN_2 and H_2 at the other. These two local conditions results in two interfaces involving

three species from reaction B. Because of the different species in equilibrium, it is likely that the interfaces will have different chemical potentials for the individual elements. The difference in chemical potentials at each interface will result in different equilibrium defect concentrations at each interface and therefore a defect migration driving force through the $Li_4BN_3H_{10}$ phase.

If we consider interface I from Figure 2 we have the following set of equilibrium conditions:

$$4\,\mu_{\mathrm{Li}} + \mu_{\mathrm{B}} + 3\,\mu_{\mathrm{N}} + 10\,\mu_{\mathrm{H}} = E_{\mathrm{Li_4BN_3H_{10}}} \tag{2}$$

$$\mu_{\mathrm{Li}} + \mu_{\mathrm{N}} + 2\,\mu_{\mathrm{H}} = E_{\mathrm{LiNH_2}} \tag{3}$$

$$\mu_{\mathrm{H}} = \frac{1}{2} E_{\mathrm{H_2}} \tag{4}$$

With only three species in equilibrium at an interface, we do not have enough equilibrium conditions to solve uniquely for the chemical potentials (i.e. an underdetermined system), and end up with one chemical potential being 'free'. In order for any results based on these chemical potentials to have relevance to the system at hand, we must be able to constrain this free potential in some way. We chose to constrain the nitrogen chemical potential, μ_{N}, based on the following equilbrium condition:

$$\mu_{\mathrm{N}} + 3\mu_{\mathrm{H}} = E_{\mathrm{NH_3}} \tag{5}$$

Although this choice is admittedly arbitrary, we chose this condition because some NH_3 release is observed experimentally during decomposition that nominally proceeds according to reaction B[7]. Additionally, we consider the free energies associated with the gas-phase species H_2 and NH_3 to be functions of temperature and pressure. The resulting local equilibria are illustrated schematically in Figure 3b.

Reaction A is over-constrained (i.e. more equations than unknowns) due to having five species in the reaction. For this reaction, we can construct four-phase equilibria based on combinations of the compounds in the reaction[See Figure 3a]. For example, based on reaction A, we can assume an equilibrium between LiH, BN, H_2 and $Li_4BN_3H_{10}$ at one point and $LiNH_2$, BN, H_2 and $Li_4BN_3H_{10}$ at another. But we can also assume there is a point where $LiNH_2$, LiH, H_2 and $Li_4BN_3H_{10}$ are in equilibrium.

Because reaction C occurs well after $Li_4BN_3H_{10}$ has melted (it melts at 460 K[5–7]), determining the formation energies of point defects based on calculations in a crystal is not appropriate. Therefore, we do not use reaction C to determine equilibrium conditions for

our point defect calculations, restricting our discussion to the temperature range in which $Li_4BN_3H_{10}$ is solid. For completeness, and because $Li_4BN_3H_{10}$ near melting retains some degree of order[29], we also include the formation energies for conditions derived from reaction B, assuming contact with NH_3 and H_2 reservoirs at 520 K (assuming 1 bar pressure), the experimental desorption temperature[5–7]. We have summarized the reactions, the resulting chemical potentials and the external constraints applied in Table II.

Reaction		Phases in Equilibrium		Additional Conditions
A	$Li_4BN_3H_{10} \rightarrow 2\ LiNH_2 + 2\ LiH + BN + 2\ H_2$	2	$Li_4BN_3H_{10}, LiNH_2, BN, H_2$	None
		3	$Li_4BN_3H_{10}, LiH, BN, H_2$	None
		4	$Li_4BN_3H_{10}, LiH, LiNH_2, H_2$	None
B	$Li_4BN_3H_{10} \rightarrow Li_3BN_2 + LiNH_2 + 4\ H_2$	5	$Li_4BN_3H_{10}, Li_3BN_2, H_2$	$\mu_N + 3\mu_H = E_{NH_3}$
		6	$Li_4BN_3H_{10}, LiNH_2, H_2$	$\mu_N + 3\mu_H = E_{NH_3}$

TABLE II. Table of the chemical potential sets derived from the two-interface model illustrated in Figure 2, for reaction A, the chemical potentials are based on combinations of the compounds present in the reaction that result in a four way equilibrium that includes $Li_4BN_3H_{10}$ and H_2. The numbers will be used to indicate the chemical potential set in later diagrams.

E. Reference States for Chemical Potentials

In Table II, the phases that are in equilibrium at our assumed interfaces are given. We use $Li_4BN_3H_{10}$, $LiNH_2, LiH, Li_3BN_2, BN, NH_3, N_2$, and H_2 to determine the chemical potentials for each of the elements based on the equilibrium conditions given in Table II. The chemical potentials are then used to calculate the defect formation energy by substituting them into Equation 1.

The energies for $Li_4BN_3H_{10}$, $LiNH_2, LiH, Li_3BN_2, BN, NH_3$, and H_2 were determined via DFT, using the same parameters as the $Li_4BN_3H_{10}$ calculations described earlier and initial structures from the ICSD database. Each of these reported structures was fully relaxed via DFT to obtain the energy used to determine the chemical potentials. For $LiNH_2, LiH, Li_3BN_2$, and BN the ground state energies of the solid at zero pressure were used. For NH_3, and H_2, the energies used were the ground state energy of the isolated

molecule, approximated by relaxing the bonds in a single molecule contained in a 10 Å box. Additionally, to examine the variations in defect formation energy when exposed to a finite temperature hydrogen or ammonia reservoir (assuming pressure fixed at 1 bar), we added the temperature and pressure correction to the ground state energy for the H_2 and NH_3 molecules using data from the NIST JANAF database[59,60].

III. RESULTS

A. Neutral Defects

We have compiled the formation energies for the neutral vacancies and interstitials we considered in Tables III and IV. For the formation energy we consider each defect to be a single vacancy (i.e. a BH_3 vacancy and an H vacancy, etc. are considered to be 'one defect' for the units in Tables III and IV). For chemical potential set 1, at 0 K the lowest energy vacancy is a BH_3 vacancy, and we find it has a negative formation energy. A negative formation energy indicates that the system would spontaneously form defects, and therefore the assumption of local equilibrium under those conditions indicates an instability. This instability is important, as the findings of Ref. 50 rely on this chemical potential set to draw conclusions about hydrogen desorption. They found hydrogen defects to be low energy and stable (positive formation energy), but their study did not include this vacancy configuration and therefore they could not have been expected to find indications of this instability.

For the chemical potentials corresponding to interfaces based on the favored reaction at 0 K (i.e. reaction A, and chemical potentials 2-4), we see positive formation energies for all the neutral defects we considered, with NH vacancies being the lowest energy. Our results indicate that the NH vacancy formation energy for set 3 is lower than set 4, which is lower than set 2. One ramification of this difference in formation energies is that it will set up a diffusion driving force for these defects through bulk $Li_4BN_3H_{10}$, as a result of the concentration gradient between any two of these local chemical potentials. We also find that at 300 K, the upper temperature limit for reaction A, that the interface corresponding to chemical potential set 3 is unstable because the BH_3 vacancy has a negative formation energy. However, the other two interfaces (chemical potential sets 2 and 4) remain stable but now set 2 has a lower NH vacancy formation energy than set 3. This change in formation

Low Temperature Neutral Defect Formation Energies (eV/defect)							
Vacancy Type	Species in Equilibrium with $Li_4BN_3H_{10}$						
	Li_3BN_2, Li_2NH, NH_3	$LiNH_2$, BN, H_2		LiH, BN, H_2		$LiNH_2$, LiH, H_2	
	1	2		3		4	
	0 K	0 K	300 K	0 K	300 K	0 K	300 K
BH_3	**-0.76**	0.63	0.32	0.73	**-0.22**	0.58	1.06
NH_3	2.90	2.80	2.16	2.70	2.70	2.75	2.27
LiH	1.89	1.93	2.24	1.98	1.98	1.98	1.98
BN	2.16	2.20	2.20	2.20	2.20	2.10	3.06
$LiBH_4$	-0.60	0.84	0.84	0.99	0.03	0.84	1.32
$LiNH_2$	1.41	0.94	0.94	0.89	1.20	0.94	0.78
H2	2.33	2.54	2.38	2.54	2.38	2.54	2.38
H3	1.82 ($\sim 2.1^{50}$)	2.03	1.87	2.03	1.87	2.03	1.87
H_2 cnfg 1	4.69	5.11	4.79	5.11	4.79	5.11	4.79
H_2 cnfg 2	1.70	2.11	1.70	2.11	1.70	2.11	1.70
NH cnfg 1	0.91	**0.39**	**0.08**	**0.29**	0.61	**0.34**	**0.18**
H inter.	2.35	2.14	2.30	2.14	2.30	2.14	2.30

TABLE III. Formation energies for each type of neutral vacancy considered and the lowest energy hydrogen interstitial at 0 and 300 K for chemical potentials derived from reaction A and the set used in Ref. 50 (0 K only). The numbers below each heading are used in the text to refer to each set of chemical potentials. In cases where multiple configurations are shown, this refers to the removal of different hydrogen atoms as described in Figure 1 and the text. Bold text indicates the lowest energy defect for each set of chemical potentials and temperature.

energy at each interface indicates a reversal of the concentration gradient, and therefore the mass transport direction, as temperature increases.

We find that the interfaces corresponding to the experimentally observed reaction (reaction B: chemical potential sets 5 and 6) are stable at 300 K, but only set 6 is stable up to

High Temperature Neutral Defect Formation Energies (eV/defect)						
Vacancy Type	Species in Equilibrium with $Li_4BN_3H_{10}$					
	Li_3BN_2, NH_3, H_2			$LiNH_2$, NH_3, H_2		
	5			6		
	300 K	460 K	520 K	300 K	460 K	520 K
BH_3	**0.25**	**-3.51**	**-4.99**	0.56	0.45	0.41
NH_3	2.40	2.07	1.94	2.40	2.07	1.94
LiH	2.08	3.10	3.50	2.00	2.11	2.15
BN	2.38	-1.03	-2.38	2.68	2.93	3.03
$LiBH_4$	0.61	-2.13	-3.22	0.84	0.84	0.84
$LiNH_2$	1.01	1.93	2.29	0.94	0.94	0.94
H2	2.38	2.27	2.22	2.38	2.27	2.22
H3	1.87	1.75	1.71	1.87	1.75	1.71
H_2 cnfg 1	4.79	4.56	4.47	4.79	4.56	4.47
H_2 cnfg 2	1.70	1.47	1.38	1.70	1.47	1.38
NH cnfg 1	0.31	0.21	0.17	**0.31**	**0.21**	**0.17**
H inter.	2.30	2.42	2.46	2.30	2.42	2.46

TABLE IV. Formation energies for each type of neutral vacancy considered and the lowest energy hydrogen interstitial at 300, 460, and 520 K for chemical potentials derived from reaction B. Bold text indicates the lowest energy defect for each set of chemical potentials and temperature.

the experimentally reported H_2 desorption temperature (520 K). Chemical potential set 5 becomes unstable between 300 K and 460 K due to the formation energy for B-containing defects becoming negative, while the other defects remain stable. This indicates that the boron chemical potential has a strong influence on the stability of the interface. For chemical potential 6, we see that the NH vacancy is the lowest energy defect and has a positive formation energy as in sets 2 and 4 and it remains stable up to the maximum temperature for each of these equilibrium conditions.

We also find that the formation energy for some defects is the same across several chemical potential sets at the same temperature, such as the H vacancies in chemical potential sets 2-4, the $LiBH_4$ and $LiNH_2$ vacancies in chemical potential sets 2 and 6, and the NH vacancies in chemical potential sets 5 and 6. For the hydrogen defects, this invariability arises simply because their formation energies are completely determined by the equilibrium with hydrogen gas as opposed to the combination of compounds in chemical potential set 1. Similarly the formation energy of NH_3 vacancies in any chemical potential set that assumes the presence of NH_3 gas at 0 K will have the same NH_3 vacancy formation energy as chemical potential set 1 because it is defined by the energy of NH_3. The NH_3 vacancy formation energy differs in chemical potential set 5 simply due to the temperature assumed for the gas phase species. For the $LiBH_4$ and $LiNH_2$ vacancies in sets 2 and 6 the situation is slightly different: the invariance in formation energy is due to the phases in common and the assumed equilibrium conditions. Specifically, sets 2 and 6 all have $Li_4BN_3H_{10}$ and $LiNH_2$ in common and the energy of an $LiBH_4$ 'unit' can be expressed as a combination of the energies of the three common species (e.g., $E_{\mathrm{LiBH_4}} = E_{\mathrm{Li_4BN_3H_{10}}} - 3E_{\mathrm{LiNH_2}}$), which are independent of the chemical potential set and H_2/NH_3 reservoir temperature or pressure. For the NH vacancy in chemical potential sets 5 and 6, the formation energy at each temperature is the same because the chemical potentials μ_N and μ_H are both determined solely by the energy of NH_3 and H_2, which are the same in both chemical potential sets at a given temperature.

Our results show that neutral hydrogen and H_2 vacancies as well as hydrogen interstitials are among the higher energy defects considered, with formation energies over approximately 1 eV/defect, regardless of the chemical potential. This finding of high-energy hydrogen defects disagrees with the results of Ref. 50, as our results indicate there would not be significant concentrations of neutral H vacancies or interstitials compared to other defects such as NH vacancies. With that in mind, we do find that the lowest energy neutral *hydrogen* vacancy is configuration 3, in agreement with Ref. 50. Interestingly, for neutral H_2 vacancy configuration 2 we find the formation energy to be lower than some single neutral H vacancy configurations. Upon inspecting the relaxed structure of neutral H_2 vacancy configuration 2 (see Figure 4), we find that the anions from which the hydrogen atoms were removed (initially a BH_4^- and NH_2^- with a B-N distance of 4.04 Å) have come together during the course of relaxation, forming a new $[BH_3NH]^{2-}$ anion with nearly the same bond lengths as crystalline ammonia borane (BH_3NH_3)[61] and the amidoborane ion $([BH_3NH_2]^-)$[62]. The

bond lengths from our result and those in Refs. 62 and 61 are given in Table V.

	Bond Length (Å)			
Bond	$[BH_3NH]^{2-}$	$LiBH_3NH_2$[62]	$Ca(BH_3NH_2)_2$[62]	BH_3NH_3[61]
B-N	1.573	1.562	1.575	1.582
N-H	1.030	1.025	1.027/1.033	0.963/1.074
B-H	1.267/1.235/1.227	1.249	1.263/1.248/1.226	1.153/1.183

TABLE V. Comparison of the $[BH_3NH]^{2-}$ anion in Figure 4 and the experimental values for the amidoborane anion in $LiBH_3NH_2$, $Ca(BH_3NH_2)_2$[62], and crystalline BH_3NH_3[61]

B. Charged Defects

Our results for the formation energies of the charged defects we considered are given in Figures 5 through 7. Each figure corresponds to a different set of chemical potentials at the specified temperature. For brevity, we have not included chemical potential sets 3 and 5, as they become unstable in the relevant temperature range. We have included neutral hydrogen defects to provide a reference to the magnitude of the neutral defects. In each case, the charged defects have been plotted for values of the Fermi energy in the bandgap based on the perfect crystal. In the figures, V^{x^q} refers to a vacancy of species x with overall charge q and X_i^q refers to an interstitial of species X with charge q. Overall, we find the chemical potentials change not only the scale of the formation energies but also the relative ordering of the defects.

In Figure 5, we have plotted our charged defect formation energies for the chemical potential set used in Ref. 50 (chemical potential set 1 in Table III). We find that charged H interstitials are the lowest energy hydrogen defects through the entire Fermi energy range, in agreement with Ref. 50. Like Ref. 50, our calculations indicate that the most favored arrangement for H_i^+ is near an NH_2^- and results in an NH_3 molecule being formed. We find that H_i^- is most preferable when it has 2 Li^+ nearest neighbors, also in agreement with Ref. 50. We find that the favored H_i^0 arrangement also results in an NH_3 molecule being formed unlike Ref. 50, who found that a neutral H atom loosely bound to the hydrogen in a BH_4^- anion is preferred. We found their reported configuration to be higher in energy by

approximately 0.25 eV/defect than our lowest energy H_i^0 configuration. This discrepancy may simply be the result of differences between the simulation approaches used, such as the different exchange-correlation functional, energy cutoff and convergence criterion used in Ref. 50, but the exact root of this discrepancy is unclear.

Despite the general agreement with[50] for hydrogen-related defects, we find that other defects are lower in energy. If we consider all of the various charged defects plotted in Figure 5, we find that the lowest energy charged defects through the range of Fermi energies are $V^{BH_4^+}$ (for $E_F <\sim 3.16$ eV) and V^{Li^-} (for $E_F \geq\sim 3.16$ eV). The combination of these two isolated defects in a single large cell, separated but allowing the system to remain charge neutral, would have a total formation energy of approximately -0.005 eV/defect (i.e. the sum of the $V^{BH_4^+}$ and V^{Li^-} formation energies, and consider this one defect). If we compare this to the formation energy for a single neutral $LiBH_4$ vacancy (-0.60 eV/defect, given in Table III), we find that the single monolithic neutral defect has a lower formation energy. The extent to which the energy of the combined neutral vacancy is lower than the two isolated charged vacancies is the binding of the individual charged vacancies. It is reasonable to expect a favorable binding between oppositely charged defects simply due to Coulombic interactions. This trend of favorable binding holds for all pairs of charged defects for which we carried out analogous neutral defect calculations (i.e. $V^{LiNH_2{}^0}$ vs. $V^{Li^-} + V^{NH_2^+}$, etc.) and for all chemical potentials. Thus in no case, do we find charged defects to be the lowest in energy, as the combined neutral defect is always more favorable.

In Figure 6(a), we have given the charged defect formation energies for chemical potential set 2 at 300 K. We find qualitative changes in defect ordering compared to Figure 5. The shifts in formation energies relative to those seen in Figure 5 are due to the changes in the relative values of the chemical potentials in set 1 and 2, which are a result of different species being assumed to be in equilibrium as well as the temperature assumed for H_2 in the particular chemical potential set. Also recall that this chemical potential set is one of the two that correspond to the low temperature desorption reaction (reaction A). Under these conditions, the lowest energy charged defects are $V^{NH_2{}^+}$ ($E_F <\sim 2.76$ eV) and V^{Li^-} (for $E_F \geq\sim 2.76$ eV). We also find the $V^{BH_4{}^+}$ and $V^{NH_2{}^+}$ defects have nearly equal formation energies, differing by less than .05 eV/defect, indicating there may be some competition between $V^{BH_4{}^+}$ and $V^{NH_2{}^+}$ under these chemical potentials. Figure 6(b) contains our calculated charged defect formation energies for chemical potential set 4 at 300 K. Set 4

is the second stable set corresponding to the low temperature desorption reaction (reaction A). Under these conditions, $V^{NH_2{}^+}$ is the lowest energy defect for $E_F <\sim 2.57$ eV, while V^{Li^-} becomes lowest for $E_F >\sim 2.57$ eV. We find that $V^{BH_4{}^+}$ has shifted upward from its level relative to $V^{NH_2{}^+}$ in Figure 6(a), as a result of the changed chemical potentials while $V^{NH_2{}^+}$ increases by approximately 0.1 eV/defect and H_i^+ remains unchanged.

The charged defect formation energies for the stable high temperature interface are shown in Figure 7. Here we see that the lowest energy charged defects are $V^{NH_2{}^+}$ ($E_F <\sim 2.83$ eV) and V^{Li^-} ($E_F >\sim 2.83$ eV). Like chemical potential set 2, we find that the formation energies of $V^{NH_2{}^+}$ and $V^{BH_4{}^+}$ are nearly degenerate.

IV. CONCLUSIONS

We calculated the formation energies for a large set of defects (charged and neutral vacancies, and hydrogen interstitials) in $Li_4BN_3H_{10}$ for a range of temperature dependent chemical potentials using DFT. Our calculations showed that neutral NH vacancies were the lowest energy defect for nearly all of the chemical potentials we considered. In the cases where the NH vacancy was not the lowest energy, a neutral BH_3 vacancy was the lowest, and had a negative formation energy. A negative formation energy would result in spontaneous formation of a large concentration of defects, and thus indicates an instability in the associated local equilibrium conditions.

We find that the three local equilibrium conditions which correspond to the low temperature desorption reaction are thermodynamically stable at 0 K, though only two of those sets are stable at 300 K. For the two equilibrium conditions derived from the experimentally observed desorption reaction, we find that both are stable at 300 K, but only one is stable at the experimental desorption temperature. Additionally, we find that neutral H and H_2 vacancies have high positive formation energies for all of the conditions considered. Our results show that positively charged H vacancies are never the lowest energy defect in contrast to the conclusion of Ref. 50, though their study did not include defects such as NH or BH_3 vacancies. Additionally, we find that positively charged NH_2 and negatively charged Li vacancies are nearly always the lowest energy charged defect. Finally, we find that the formation energy of two isolated and oppositely charged defects is never lower than a single analogous combined neutral defect. This finding can be easily explained by Coulomb

interactions favoring the binding of oppositely charged defects, resulting in a lower energy configuration.

It is important to note that the formation energies we calculated are only part of the complete picture of mass transport in this compound, since our present results do not indicate how readily defects move once created. We believe more work is needed to assess the diffusion fluxes, migration barriers and ultimately mass transport activation energies for these defects, as has been done for $NaAlH_4$[41–43].

ACKNOWLEDGMENTS

We would like to thank Kyle Michel, Prof. Vidvuds Ozoliņš, and Yongsheng Zhang for their input during the preparation of this manuscript. This work was supported by DOE grant numbers DE-FG02-07ER46433 and DE-FC36-08G018136. This research was supported in part by the National Science Foundation through TeraGrid resources. The computations were performed in part on the Kraken system at the National Institute for Computational Sciences. This research also used the resources of the Argonne Leadership Computing Facility at Argonne National Laboratory, which is supported by the Office of Science of the U.S. Department of Energy under contract DE-AC02-06CH11357.

---

* c-wolverton@northwestern.edu

[1] S. Satyapal, J. Petrovic, C. Read, G. Thomas, and G. Ordaz, Catalysis Today **120**, 246 (2007).

[2] J. Yang, A. Sudik, C. Wolverton, and D. J. Siegel, Chemical Society Reviews **39** (2010).

[3] G. Alefeld and J. Völkl, eds., *Hydrogen in Metals II, Application-oriented properties*, Topics in Applied Physics, Vol. 29 (Springer-Verlag, 1978).

[4] S. Orimo, Y. Nakamori, J. Eliseo, A. Züttel, and C. Jensen, Chemical Reviews , 4111 (2007).

[5] F. Pinkerton, G. Meisner, M. S. Meyer, M. Balogh, and M. Kundrat, Journal of Physical Chemistry B **109**, 6 (2005).

[6] Y. Filinchuk, K. Yvon, G. Meisner, F. Pinkerton, and M. Balogh, Inorganic Chemistry **45**, 1433 (2006).

[7] F. Pinkerton and M. Meyer, Journal of Physical Chemistry C **113**, 11172 (2009).

[8] P. Chater, W. David, S. Johnson, P. Edwards, and P. Anderson, Chemical Communications , 2439 (2006).

[9] T. Noritake, M. Aoki, S. Towata, A. Ninomiya, Y. Nakamori, and S. Orimo, Applied Physics A **83**, 277 (2006).

[10] J. P. Singer, M. Meyer, R. Speer, J. Fisher, and F.E.Pinkerton, Journal of Physical Chemistry C **113**, 18927 (2009).

[11] D. J. Siegel, C. Wolverton, and V. Ozoliņš, Physical Review B **75**, 014101 (2007).

[12] C. Wolverton, V. Ozoliņš, and M. Asta, Physical Review B **69**, 144109 (2004).

[13] A. Akbarzadeh, V. Ozoliņš, and C. Wolverton, Advanced Materials **19**, 3233 (2007).

[14] S. Alapati, J. Johnson, and D. Sholl, Physical Chemistry Chemical Physics **9**, 1438 (2007).

[15] C. Wolverton, D. Siegel, A. Akbarzadeh, , and V. Ozoliņš, Journal of Physics: Condensed Matter **20**, 064228 (2008).

[16] S. Shevlin and Z. Guo, Chemical Society Reviews **38**, 211 (2009).

[17] K. Kim, A. Anant, J. Johnson, and D. Sholl, Physical Chemistry Chemical Physics **13**, 7218 (2011).

[18] Z. Łodziana and T. Vegge, Physical Review Letters **93**, 145501 (2004).

[19] E. Majzoub, K. McCarty, and V. Ozoliņš, Physical Review B **71**, 024118 (2005).

[20] T. Vegge, Physical Chemistry Chemical Physics **8**, 4853 (2006).

[21] K. Miwa, N. Ohba, S. Towata, Y. Nakamori, and S. Orimo, Physical Review B **71**, 195109 (2005).

[22] B. Magyari-Köpe, V. Ozoliņš, and C. Wolverton, Physical Review B **73**, 220101(R) (2006).

[23] T. Mueller and G. Ceder, Physical Review B **74**, 134104 (2006).

[24] C. Wolverton and V. Ozoliņš, Physical Review B **75**, 064101 (2007).

[25] Z. Ma and M. Chou, Journal of Applied Physics **104**, 083519 (2008).

[26] Y. Lee, Y. Kim, Y. Cho, D. Shapiro, C. Wolverton, and V. Ozoliņš, Physical Review B **79**, 104107 (2009).

[27] J. Herbst and L. H. Jr., Applied Physics Letters **88**, 231904 (2006).

[28] H. Wu, W. Zhou, T. Udovic, J. Rush, and T. Yildirim, Chemistry of Materials **20**, 1245 (2008).

[29] D. Farrell, D. Shin, and C. Wolverton, Physical Review B **80**, 224201 (2009).

[30] V. Ozoliņš, E. Majzoub, and C. Wolverton, Physical Review Letters **100**, 135501 (2008).

[31] A. Bil, B. Kolb, R. Atkinson, D. G. Pettifor, T. Thonhauser, and A. N. Kolmogorov, Physical Review B **83**, 224103 (2011).

[32] Y. Zhang, E. Majzoub, V. Ozoliņš, and C. Wolverton, Physical Review B **82**, 174107 (2010).

[33] W. Sun, C. Wolverton, A. Akbarzadeh, and V. Ozoliņš, Physical Review B **83**, 064112 (2011).

[34] F. Zhang, Y. Wang, and M. Chou, Physical Review B **83**, 012101 (2011).

[35] C. Weidenthaler, A. Pommerin, M. Felderhoff, W. Sun, C. Wolverton, B. Bogdanovic, and F. Schuth, Journal of the American Chemical Society **131**, 16735 (2009).

[36] C. Kim, S.-J. Hwang, R. C. Bowman, J. W. Reiter, J. A. Zan, J. G. Kulleck, H. Kabbour, E. H. Majzoub, and V. Ozolins, Journal of Physical Chemistry C **113**, 9956 (2009).

[37] T. Noritake, M. Aoki, M. Matsumoto, K. Miwa, S. Towata, H. W. Li, and S. Orimo, Journal of Alloys and Compounds **509**, 7553 (2011).

[38] D. Aidhy, Y. Wang, and C. Wolverton, Physical Review B **84**, 134103 (2011).

[39] V. Ozoliņš, E. Majzoub, and C. Wolverton, Journal of the American Chemical Society **131**, 230 (2009).

[40] A. Kulkarni, L. Wang, D. Johnson, D. Sholl, and J. Johnson, Journal of Physical Chemistry C **114**, 14601 (2010).

[41] K. Michel and V. Ozoliņš, Journal of Physical Chemistry C **115**, 21443 (2011).

[42] K. Michel and V. Ozoliņš, Journal of Physical Chemistry C **115**, 21465 (2011).

[43] K. Michel and V. Ozoliņš, Journal of Physical Chemistry C **115**, 21454 (2011).

[44] A. Peles and C. V. de Walle, Physical Review B **76**, 214101 (2007).

[45] Z. Lodziana, A. Züttel, and P. Zielinski, Journal of Physics: Condensed Matter **20**, 465210 (2008).

[46] H. Gunaydin, K. Houk, and V. Ozoliņš, Proceedings of the National Academy of Science **105**, 3673 (2008).

[47] A. Tekin, J. S. Hummelshoj, H. S. Jacobsen, D. Sveinbjornsson, D. Blanchard, J. K. Norskov, and T. Vegge, Energy & Environmental Science **3**, 448 (2010).

[48] L. Ismer, A. Janotti, and C. V. de Walle, Applied Physics Letters **97**, 201902 (2010).

[49] D. Blanchard, M. D. Riktor, J. B. Maronsson, H. S. Jacobsen, J. Kehres, D. Sveinbjornsson, E. G. Bardaji, A. Leon, F. Juranyi, J. Wuttke, B. C. Hauback, M. Fichtner, and T. Vegge, Journal of Physical Chemistry C **114**, 20249 (2010).

[50] K. Hoang and C. V. de Walle, Physical Review B **80**, 214109 (2009).

[51] G. Kresse and J. Hafner, Physical Review B **47**, 558 (1993).

[52] G. Kresse and J. Hafner, Physical Review B **49**, 14251 (1994).

[53] G. Kresse and J. Furthmüller, Computational Materials Science **6**, 15 (1996).

[54] G. Kresse and J. Furthmüller, Physical Review B **54**, 11169 (1996).

[55] G. Kresse and D. Joubert, Physical Review B **59**, 1758 (1999).

[56] J. Perdew and Y. Wang, Physical Review B **45**, 13244 (1992).

[57] P. Blöchl, Physical Review B **50**, 17953 (1994).

[58] C. V. de Walle and J. Neugebauer, Journal of Applied Physics **95**, 3851 (2004).

[59] K. Reuter and M. Scheffler, Physical Review B **65**, 035406 (2001).

[60] D. Stull and H. Prophet, *JANAF Thermochemical Tables*, 2nd ed. (US National Bureau of Standards, Washington D.C., 1971).

[61] W. Klooster, T. Koetzle, P. Siegbahn, T. Richardson, and R. Crabtree, Journal of the American Chemical Society **121**, 6337 (1999).

[62] H. Wu, W. Zhou, and T. Yildirim, Journal of the American Chemical Society **130**, 14834 (2008).

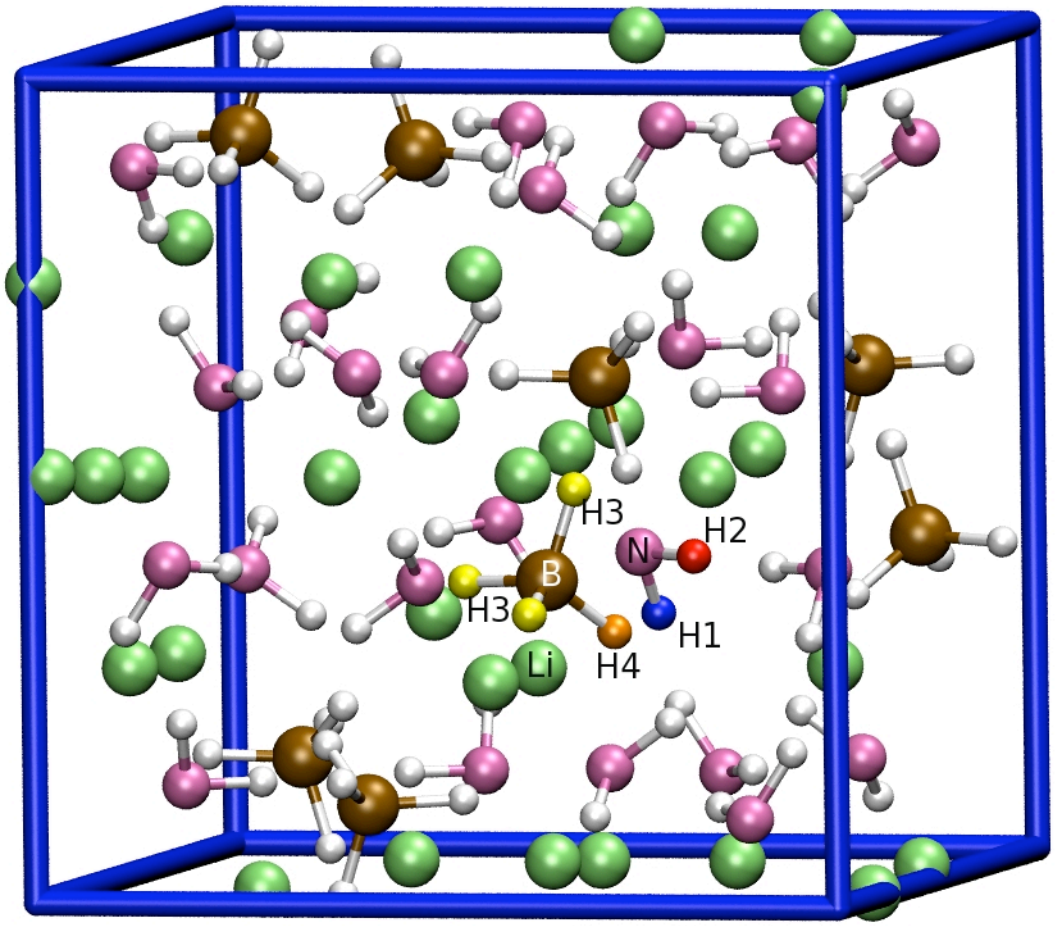

FIG. 1. The crystal structure of $Li_4BN_3H_{10}$. The letters indicate the species and the numbers indicate symmetrically inequivalent hydrogen sites. There are two distinct H positions in the NH_2^- anions (labeled H1 and H2), and in each BH_4^- anion, 3 of the H positions are of type H3, and the fourth is of type H4. The lattice parameter is approximately 10.6 Å. In the color version the unlabeled atoms are also color-coded by species: green indicates Li, pink indicates N, brown indicates B, and white indicates H.

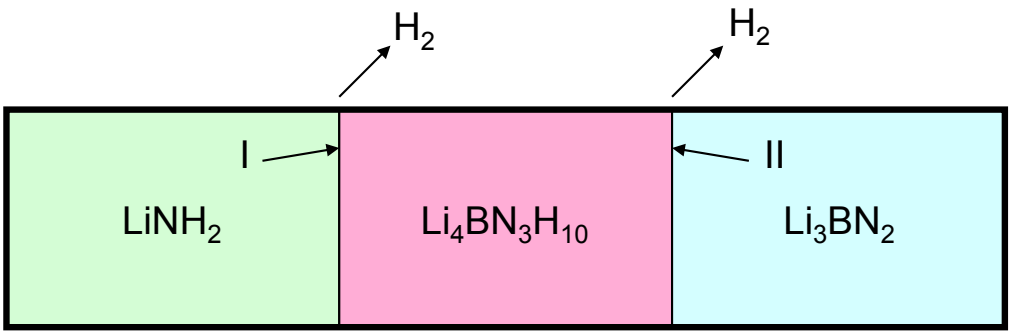

FIG. 2. Example of the interface model used to formulate chemical potentials, based on reaction B. Here, bulk $Li_4BN_3H_{10}$ is considered to be in thermodynamic equilibrium with bulk $LiNH_2$ and H_2 at interface I, and Li_3BN_2 and H_2 at interface II.

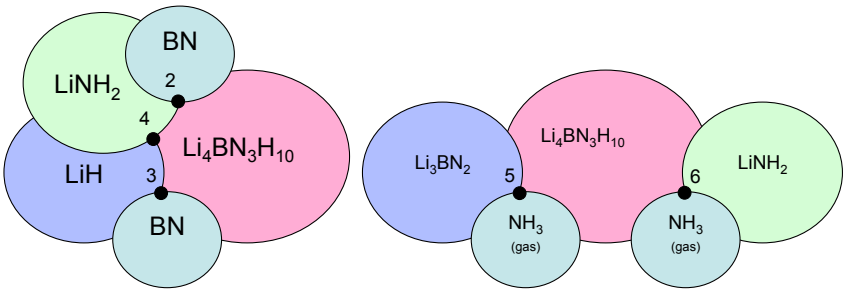

(a)Reaction A (b)Reaction B

FIG. 3. Schematic of equilibrium points represented by the chemical potential sets. H_2 is assumed to be in contact with each point. For reaction A, we have three possible four-phase equilibrium points (that include $Li_4BN_3H_{10}$ and and H_2), while reaction B results in two. The numbers indicate the number of the chemical potential set used in the text.

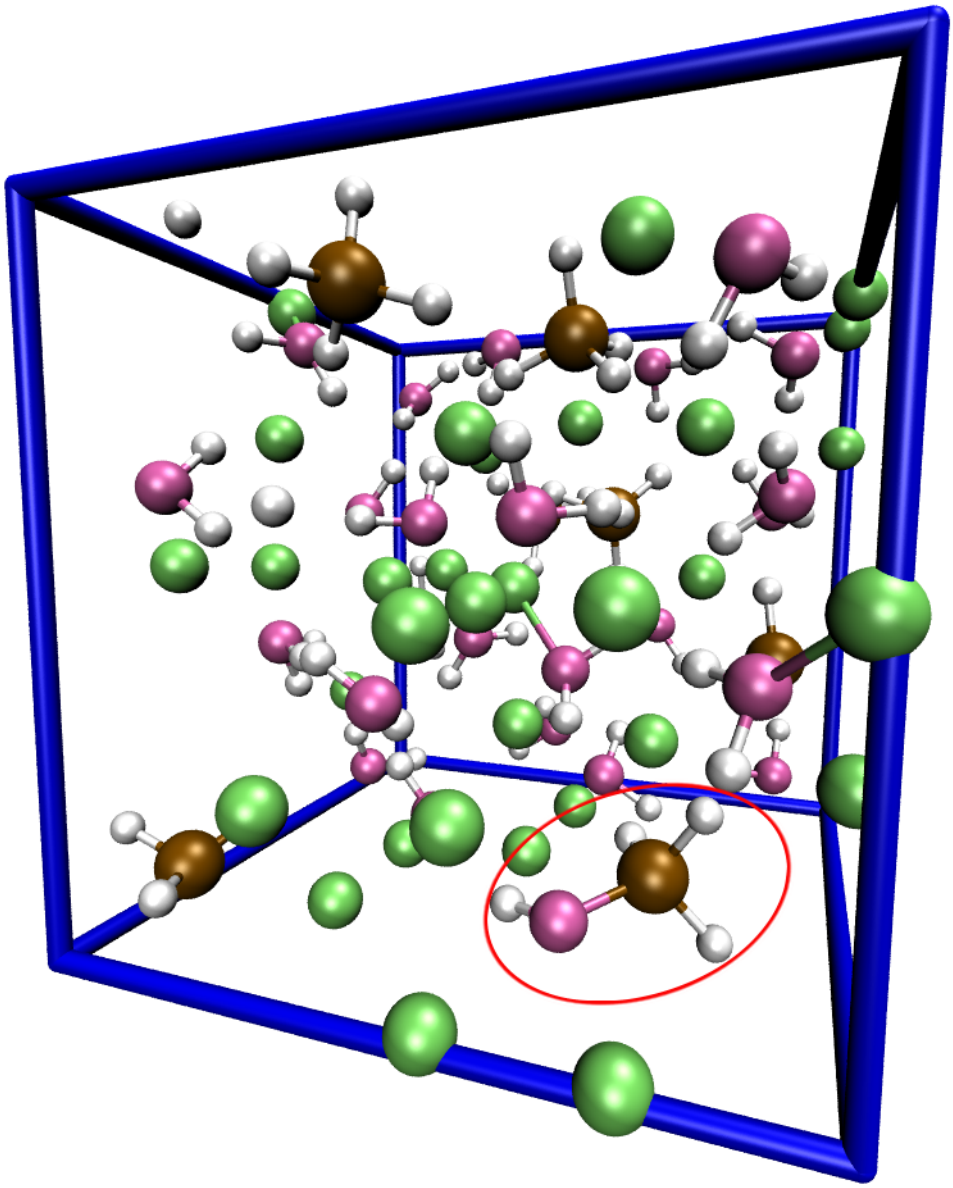

FIG. 4. The relaxed structure of neutral H_2 vacancy configuration 2. The anions from which the hydrogens were removed (initially BH_4^- and NH_2^-, circled) have come together forming a new $[BH_3NH]^{2-}$ anion.

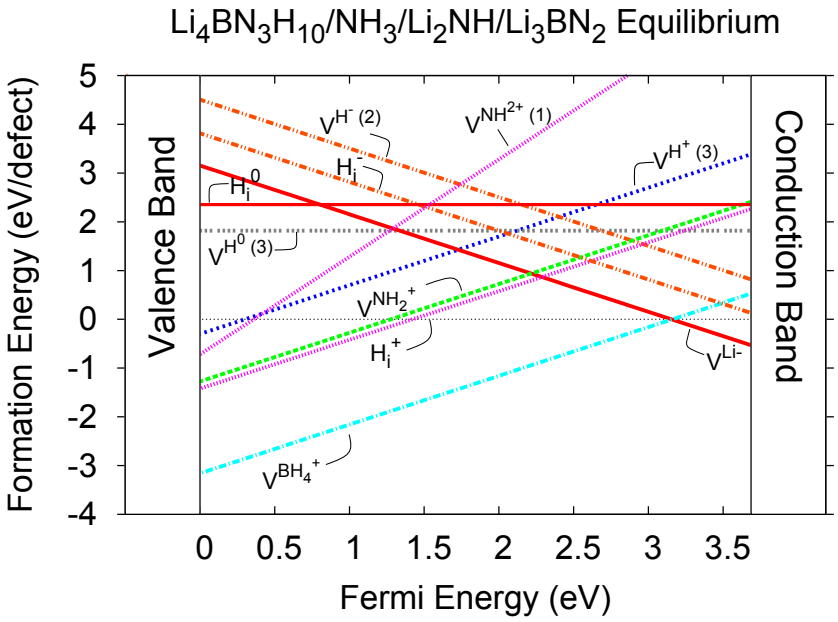

FIG. 5. Defect formation energies as a function of the Fermi Energy, assuming equilibrium between $Li_4BN_3H_{10}$, Li_3BN_2, Li_2NH, and NH_3(chemical potential set 1) at 0 K. In this and the following figures, V^{x^q} refers to a vacancy of x type with overall charge q and X_i^q refers to an interstitial of x type with charge q.

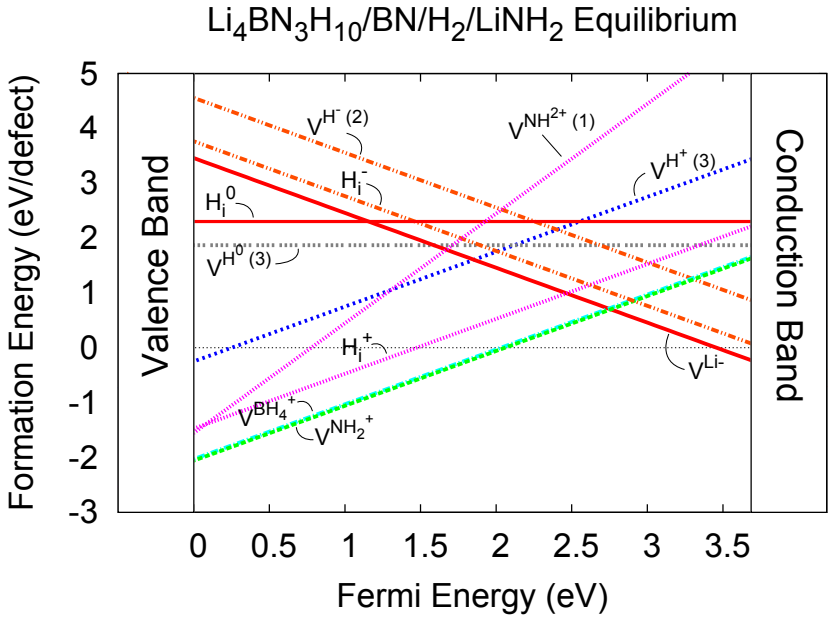

(a)Chemical Potential Set 2

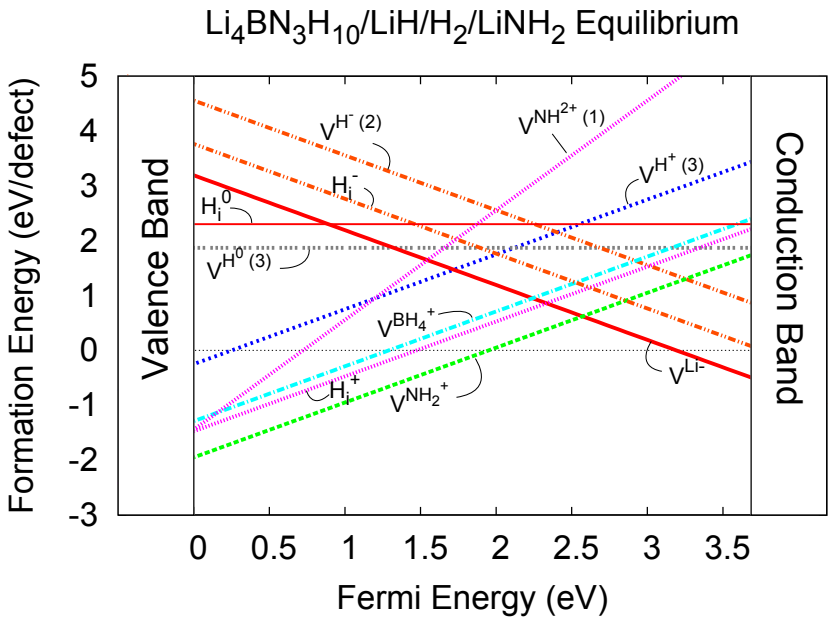

(b)Chemical Potential Set 4

FIG. 6. Defect formation energies as a function of the Fermi Energy, for chemical potential sets 2 (a) and 4 (b) at 300 K and 1 bar H_2. In (a), the lines corresponding to $V^{NH_2^+}$ and $V^{BH_4^+}$ nearly overlay one another.

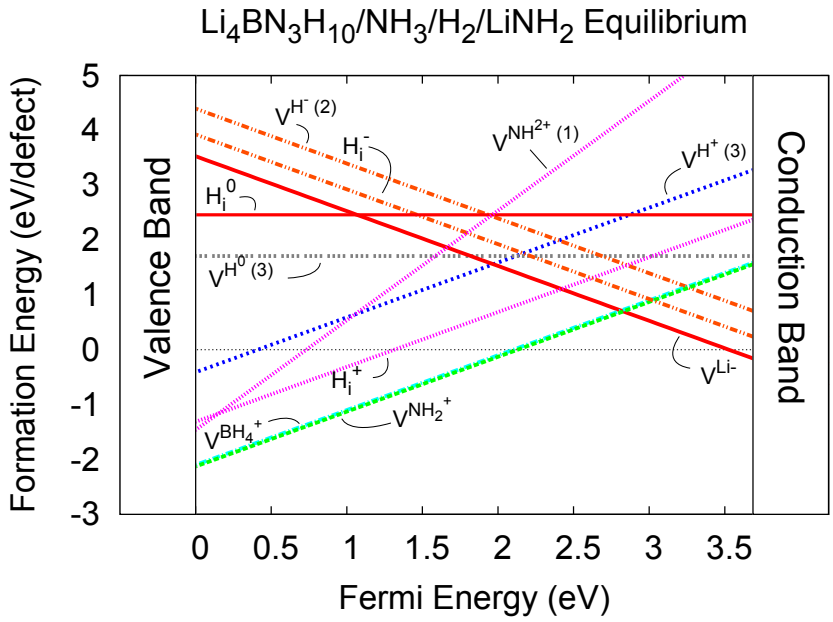

FIG. 7. Defect formation energies as a function of Fermi Energy, for chemical potential set 6 at 520 K and 1 bar H_2 and NH_3. Lines corresponding to $V^{NH_2^+}$ and $V^{BH_4^+}$ overlay one another.